Asian monsoon hydrometeorology from TES and SCIAMACHY water vapor isotope measurements and LMDZ simulations: Implications for speleothem climate record interpretation

Jung-Eun Lee, Camille Risi, Inez Fung, John Worden, Remco A. Scheepmaker, Benjamin Lintner, Christian Frankenberg

HAL Id: hal-01110325

https://hal.archives-ouvertes.fr/hal-01110325

Submitted on 27 Jan 2015

Asian monsoon hydrometeorology from TES and SCIAMACHY water vapor isotope measurements and LMDZ simulations: Implications for speleothem climate record interpretation

Jung-Eun Lee,[1] Camille Risi,[2] Inez Fung,[3] John Worden,[1] Remco A. Scheepmaker,[4] Benjamin Lintner,[5] and Christian Frankenberg[1]

[1]   Observations show that heavy oxygen isotope composition in precipitation ($\delta^{18}O_p$) increases from coastal southeastern (SE) China to interior northwestern (NW) China during the wet season, contradicting expectations from simple Rayleigh distillation theory. Here we employ stable isotopes of precipitation and vapor from satellite measurements and climate model simulations to characterize the moisture processes that control Asian monsoon precipitation and relate these processes to speleothem paleoclimate records. We find that $\delta^{18}O_p$ is low over SE China as a result of local and upstream condensation and that $\delta^{18}O_p$ is high over NW China because of evaporative enrichment of ^{18}O as raindrops fall through dry air. We show that $\delta^{18}O_p$ at cave sites over southern China is weakly correlated with upstream precipitation in the core of the Indian monsoon region rather than local precipitation, but it is well-correlated with the $\delta^{18}O_p$ over large areas of southern and central China, consistent with coherent speleothem $\delta^{18}O_p$ variations over different parts of China. Previous studies have documented high correlations between speleothem $\delta^{18}O_p$ and millennial timescale climate forcings, and we suggest that the high correlation between insolation and speleothem $\delta^{18}O_p$ in southern China reflects the variations of hydrologic processes over the Indian monsoon region on millennial and orbital timescales. The $\delta^{18}O_p$ in the drier part (north of ~30°N) of China, on the other hand, has consistently negative correlations with local precipitation and may capture local hydrologic processes related to changes in the extent of the Hadley circulation.

1. Introduction

[2] Only one-third of the Intergovernmental Panel on Climate Change Fourth Assessment Report (IPCC AR4) models capture the current seasonal and interannual variations of monsoon climate [*Annamalai et al.*, 2007], reflecting the difficulty of unraveling various processes in the hydrological cycle over the Asian monsoon region. Measurements of the isotopic composition of water can be useful in identifying controls on the hydrological cycle, e.g., source water for evapotranspiration [*Dawson and Ehleringer*, 1998], condensation altitude in the atmosphere [*Lee et al.*, 2009b], and the degree of mixing in the atmosphere [*Risi et al.*, 2012a]. Moreover, stable isotopes are recorded in paleoproxies—ice sheets, speleothems, soil carbonates, leaf waxes, animal shells or bones—and are used to infer past climatic conditions through applications of relationships between stable isotopic composition and environmental conditions [e.g., *Wang et al.*, 2001, 2008; *Rowley et al.*, 2001; *Garzione et al.*, 2006].

[3] Stable isotope values in precipitation $\delta^{18}O_p$ or δD is defined as $(R_p/R_{SMOW} - 1)$, where R_p is the isotope number ratio N_{18_O}/N_{16_O} or N_D/N_H in precipitation and R_{SMOW} represents the isotope number ratio in Standard Mean Ocean Water. The $\delta^{18}O_p$ decreases as air parcels move away from their evaporative source regions because precipitation has higher $^{18}O/^{16}O$ ratios than the original water vapor, thereby decreasing the $^{18}O/^{16}O$ ratio of the remaining vapor due to $H_2^{18}O$'s lower saturation vapor pressure (Rayleigh distillation [*Dansgaard*, 1964]). Global distributions of $\delta^{18}O_p$, in particular the observed decrease of $\delta^{18}O_p$ with decreasing temperatures from the subtropical to the polar region, have been explained by the Rayleigh distillation model. On the

_____

[1]Jet Propulsion Laboratory, California Institute of Technology, Pasadena, California, USA.
[2]LMD/IPSL, CNRS, Paris, France.
[3]Department of Earth and Planetary Science, University of California, Berkeley, California, USA.
[4]SRON Netherlands Institute for Space Research, Utrecht, Netherlands.
[5]Department of Environmental Sciences, Rutgers, State University of New Jersey, New Brunswick, New Jersey, USA.

Corresponding author: J.-E. Lee, Jet Propulsion Laboratory, California Institute of Technology, 4800 Oak Grove Dr., MS 233-200, Pasadena, CA 91109, USA. (jung-eun.lee@jpl.nasa.gov)
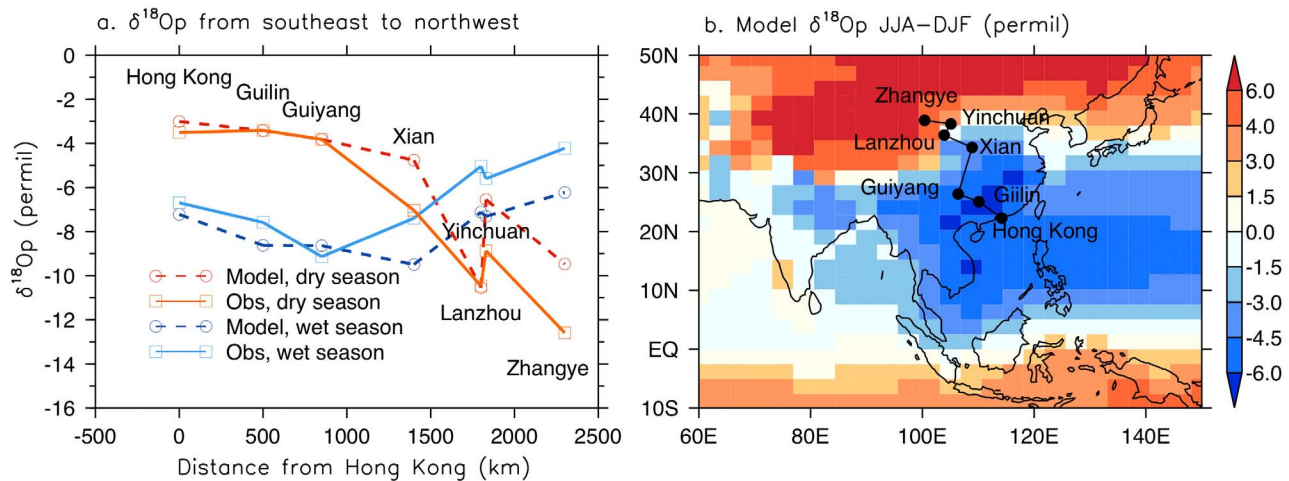
Figure 1. (a) The distribution of $\delta^{18}O_p$ from Hong Kong to Zhangye during wet (blue) and dry (red) seasons. Observations are from the Global Network for Isotopes in Precipitation (GNIP) [*Aragúas-Aragúas et al.*, 1998], and the definition of wet and dry seasons for each station also follows *Aragúas-Aragúas et al.* [1998]. For most stations, the wet season is from May to September, and the dry season is from October to April. Solid lines represent observations, and dashed lines represent model simulations. (b) The $\delta^{18}O_p$ difference between summer (JJA) and winter (DJF) from model simulations.

other hand, the recharge of moisture through evaporation outside of the major evaporation source regions (subtropical oceanic regions) increases the heavy isotope composition in atmospheric vapor ($\delta^{18}O_v$), resulting in higher $\delta^{18}O_p$ compared with no evaporative recharge conditions [*Hendricks et al.*, 2000]. Thus, the variation of the mean $\delta^{18}O_v$ over the ocean is small because of high evaporation from the ocean [*Lee et al.*, 2008].

[4] The $\delta^{18}O_p$ over Asia increases from the coast toward interior continental sites during the wet season, April through September for most of the Asian monsoon region [*Aragúas-Aragúas et al.*, 1998] (see Figure 1a), contradicting expectations from the Rayleigh distillation theory. This relationship is characterized by low $\delta^{18}O_p$ over southeastern (SE) China and high $\delta^{18}O_p$ over northwestern (NW) China. The low $\delta^{18}O_p$ over SE China has been explained by the "amount effect," the inverse relationship between $\delta^{18}O_p$ and precipitation amount as observed over tropical island stations [*Rozanski et al.*, 1993], linking the high precipitation and low $\delta^{18}O_p$ there, although the local $\delta^{18}O_p$ over the Asian monsoon is not directly related to local precipitation [*Dayem et al.*, 2010]. *Aragúas-Aragúas et al.* [1998] argue that the increase of $\delta^{18}O_p$ from coastal regions to the interior of Asia arises from different air mass origins for NW and SE China, but process-based explanations are lacking. In a paleoclimate context, detailed understanding of $\delta^{18}O_p$ over SE China and NW China is important because $\delta^{18}O_p$ from speleothems has been used to infer historical variability of the Asian monsoon during the past couple of hundred thousand years [e.g., *Wang et al.*, 2001, 2008].

[5] In this study, we examine how $\delta^{18}O$ in either vapor or precipitation can inform mechanistic understanding of the hydrological cycle over Asia, in particular focusing on why $\delta^{18}O_p$ increases from the coastal SE China to the continental interior (NW China) during the summer wet season. We first show that the relationship expected from Rayleigh distillation theory—the decrease of $\delta^{18}O_p$ from the coast to the

interior—in fact holds during winter dry season and describe the conditions under which this relationship applies. We next investigate the distinct controls on $\delta^{18}O_p$ over SE China and NW China during the summer monsoon season. We present two hypotheses for the relatively high $\delta^{18}O_p$ values prevailing over NW China: (1) rain re-evaporation over the drier continental interior and (2) a higher recycling ratio [see *Kurita and Yamada*, 2008; *Frankenberg et al.*, 2009]. We use the Laboratoire de Météorologie Dynamique Zoom model version 4 (LMDZ4) [*Hourdin et al.*, 2006] to characterize the processes controlling $\delta^{18}O_p$ over SE and NW China. We then explore the aforementioned hypotheses using observed isotopic composition of atmospheric vapor from two satellites. Finally, we discuss the implications of our findings for the interpretation of paleoproxies.

2. Methods

2.1. Model Description

[6] To understand the evolution and control of spatial and seasonal isotopic variations, we analyze results from an isotope-enabled simulation of LMDZ4. This model version incorporates the entire cycle of stable water isotopes ($\delta^{18}O_p$ and δD), with fractionation included when phase changes occur. To better reproduce the observed circulation pattern, simulated winds from LMDZ4 are relaxed toward the pseudo-observed horizontal wind field from the ERA-40 reanalysis results [*Uppala et al.*, 2005] with a time constant of 1 h. Such nudging leads to more realistic simulations of the hydrology and isotope values compared with free-running simulations [*Yoshimura et al.*, 2008; *Sturm et al.*, 2005; *Risi et al.*, 2010a]. The resolution of the model is $2.5° \times 3.75°$ with 19 vertical levels in the atmosphere. Further details of LMDZ4 and the inclusion of isotopes are given in *Hourdin et al.* [2006] and *Risi et al.* [2010a]. We integrated the LMDZ4 using observed sea surface temperatures and sea ice

fractions from the HadISST data set [*Rayner et al.*, 2003] from 1958 to 2009 as boundary conditions.

[7] In addition, we analyze results of a tagging experiment to quantify the contribution of evapotranspiration from the land surface to precipitation [e.g., *Koster et al.*, 1986]. In this experiment, two passive water tracers, one for land and one for ocean, are tracked along the LMDZ4 hydrological cycle: these tracers behave similar to water except the land tracer evaporates over land only and oceanic tracer evaporates over ocean only and move through the entire hydrologic cycle. From these tracers, we can deduce the contribution of land evapotranspiration to the total precipitation. This experiment is described in more detail in *Risi et al.* [2010b].

2.2. Data

[8] We analyze independent isotope retrievals from two satellite instruments: the Tropospheric Emission Spectrometer (TES) onboard NASA's Aura; and the Scanning Imaging Absorption Spectrometer for Atmospheric Chartography (SCIAMACHY) on board the European Space Agency's (ESA's) Environmental Research Satellite (ENVISAT). TES has a spatial footprint of 5.3×8.3 km and measures trace concentration in the mid-troposphere between 400 to 850 hPa. We use the data from *Worden et al.* [2006] with bias correction of $\sim$5‰ in the HDO/H$_2$O ratio compared with in situ observations at Mauna Loa Observatory [*Worden et al.*, 2011] averaged between 400 and 850 hPa from 2003 to 2008. SCIAMACHY retrieves the short-wave infrared (2355 to 2375 nm retrieval window), has a spatial footprint of 120×30 km, and is sensitive to the entire atmospheric column. Because the scale height of water vapor is small, the lower atmosphere (0–2 km) contributes most strongly to the SCIAMACHY HDO/H$_2$O retrieval. We analyze monthly averages from 2003 through 2005. More information on the comparison between satellite measurements and model results is described in *Risi et al.* [2012b].

[9] Although LMDZ4 captures the spatiotemporal variations of both satellite measurements, an offset of approximately +30‰ exists relative to both TES and SCIAMACHY measurements, similar to the offset evident in the isotope-enabled ECHAM5 [*Werner et al.*, 2011]. We speculate that this bias stems from the uncertainties in physics or parameterizations of the model, e.g., the atmospheric water vapor advection [*Risi et al.*, 2012b] or convection [*Lee et al.*, 2009b] schemes could introduce biases in vapor isotope simulations. In addition, there may be unresolved biases in satellite measurements, e.g., a 3% error in absorption line strength of either HDO or H$_2$O can explain a 30‰ bias. Some bias mitigation is likely to occur as additional airplane isotope measurements become available to validate satellite products. We focus on the variations of TES and SCIAMACHY in comparison with the LMDZ4 results since variations within data products are expected to be robust.

[10] We also use the Global Network of Isotopes in Precipitation (GNIP) data to evaluate our model results. GNIP data were collected by the International Atomic Energy Agency (IAEA), in cooperation with the World Meteorological Organization (WMO) beginning in 1961. These data provide a global survey of the isotopic composition in precipitation (deuterium, ^{18}O, and tritium) [*Rozanski et al.*, 1993] and have contributed greatly to our understanding of the global water isotope distribution [e.g., *Dansgaard*,

1964; *Rozanski et al.*, 1993]. All values reported here are precipitation amount-weighted mean isotopic compositions as reported in *Aragúas-Aragúas et al.* [1998].

2.3. Analysis

[11] We compare and contrast the isotope behavior in two areas of interest: the southeastern part of China (20°N–35°N, 100°E–120°E; SE China; black box in Figure 2) and the northwestern part of China (35°N–45°N, 80°E–100°E; NW China; green box in Figure 2). Over SE China, SCIAMACHY has 124 observations, with a standard error in δD of 4.9‰; TES has 2309 observations with <1‰ standard error. The number of SCIAMACHY observations over SE China is low because cloudy scenes are discarded. Over NW China, SCIAMACHY has 4393 observations and standard error of 1.1‰; TES has 456 observations with ~1.5‰ standard error. In what follows, we emphasize δ^{18}O as it is more widely reported in paleoproxy literature. However, since the satellites cannot reliably retrieve δ^{18}O, δD is shown for satellite measurements, noting that δD variations are approximately 8 times larger than δ^{18}O variations.

3. Results and Discussion

[12] Since δ^{18}O$_p$ integrates processes in the hydrological cycle—local and remote sources of water vapor from evaporation and transpiration, horizontal and vertical mixing, and phase transitions among ice, liquid, and vapor— it is necessary to obtain reasonable simulation of multiple features of the hydrological cycle to explain the controls on δ^{18}O$_p$. We thus compare precipitation simulated by LMDZ and measured by TRMM (Figures 2a–2d). Spatial correlation coefficients between TRMM and the nudged LMDZ simulation are high, 0.68 and 0.86 for summer and winter, respectively, over all grids in the domain covering 0–40°N, 60°E–120°E (Figures 2g and 2h). Seasonally, precipitation is high during boreal spring and summer and low during winter over most of the East Asian monsoon region; spatially, precipitation values decrease away from the coast. However, we point out that the model does not capture all the details of the wet season precipitation variability, while dry season precipitation near Tibet is too high [*Gao et al.*, 2011].

[13] The spatial and seasonal variations in simulated δ^{18}O$_p$ appear to be reasonable for both wet and dry seasons when compared with observations from the GNIP network [*Aragúas-Aragúas et al.*, 1998]. To illustrate the model performance, we present cross-sections of δ^{18}O$_p$ from Hong Kong to Zhangye for both the LMDZ4 simulation and GNIP observations (Figure 1a) both precipitation-amount-weighted δ^{18}O$_p$. The model captures the winter δ^{18}O$_p$ decrease toward the northwest as well as the seasonal summer increase, although some details do not match observations, e.g., the isotope values at Xian (108.9°E, 34.3°N) are in the middle of SE and NW China values in observations, but are closer to SE China values in the model. Of course, Xian lies in a hydroclimatic transition region between the humid SE and more arid NW, so the isotopic values here likely reflect strong sensitivity to the details of the hydroclimatic gradient. The spatial resolution of the model may be especially critical in this region.

[14] Evaporation over ocean increases δ^{18}O$_v$ because evaporated moisture typically has a higher isotopic composition
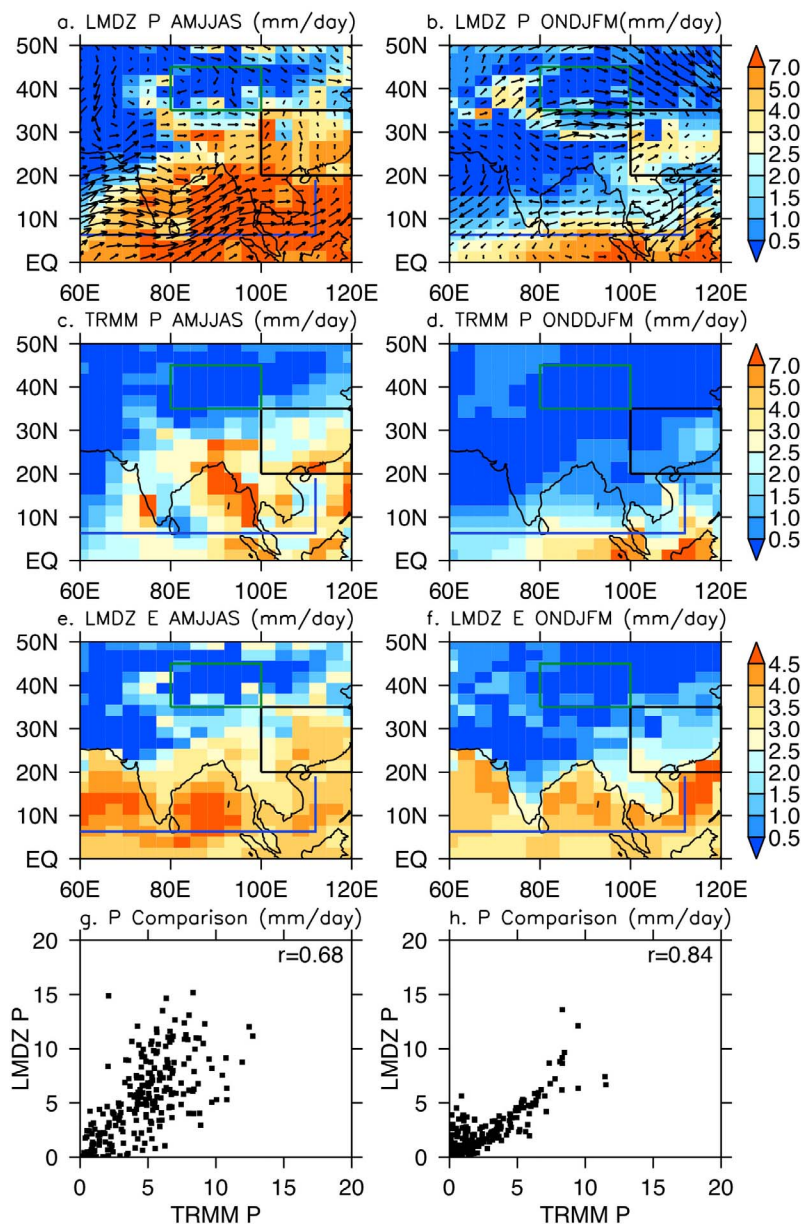
Figure 2. Mean seasonal precipitation from (a and b) model simulations, (c and d) TRMM, and (e and f) mean seasonal evapotranspiration from the surface, and the scatterplot between TRMM and LMDZ precipitation over 0–40°N and 60°E–120°E for the wet season (April through September; left column) and during the dry season (October through March; right column). Wind vectors in Figures 2a and 2b are from LMDZ model results at 900 hPa.

($\delta^{18}O_e$) than the ambient atmospheric vapor (Figures 3a and 3c) [see *Lee et al.*, 2007]. We point out that evaporation is a non-equilibrium diffusive process following the gradients of $H_2^{16}O$ or $H_2^{18}O$ vapor pressure just above the evaporating surface. Therefore, $\delta^{18}O_e$ exceeds $-10‰$ (the approximate equilibrium value with SMOW) over most of the oceanic region and can sometimes be higher than 0‰ when $H_2^{18}O$ gradients are steep (Figure 3a) [*Craig and Gordon*, 1965; *Lee et al.*, 2007]. Land transpiration also enriches the vapor in the lower troposphere because plants do not fractionate soil water during uptake [*Dawson and Ehleringer*, 1998; *Kurita and Yamada*, 2008; *Frankenberg et al.*, 2009]. Because of

mass conservation, the global mean isotopic composition of precipitation and evaporation should be almost identical, i.e., $-5.8‰$ for both in the LMDZ4 simulation.

3.1. Winter Conditions

[15] During winter, temperatures over China decrease from the coast inland, and $\delta^{18}O_p$ mirrors this decrease, consistent with expectations from the Rayleigh distillation model, i.e., the so-called "temperature effect" (Figures 1a and 3h) [*Dansgaard*, 1964]. From Xian to locations further inland (34°N), snow becomes the dominant form of precipitation because the temperature is close to or lower than 0°C. Given its low diffusivity, snow does not interact with atmospheric
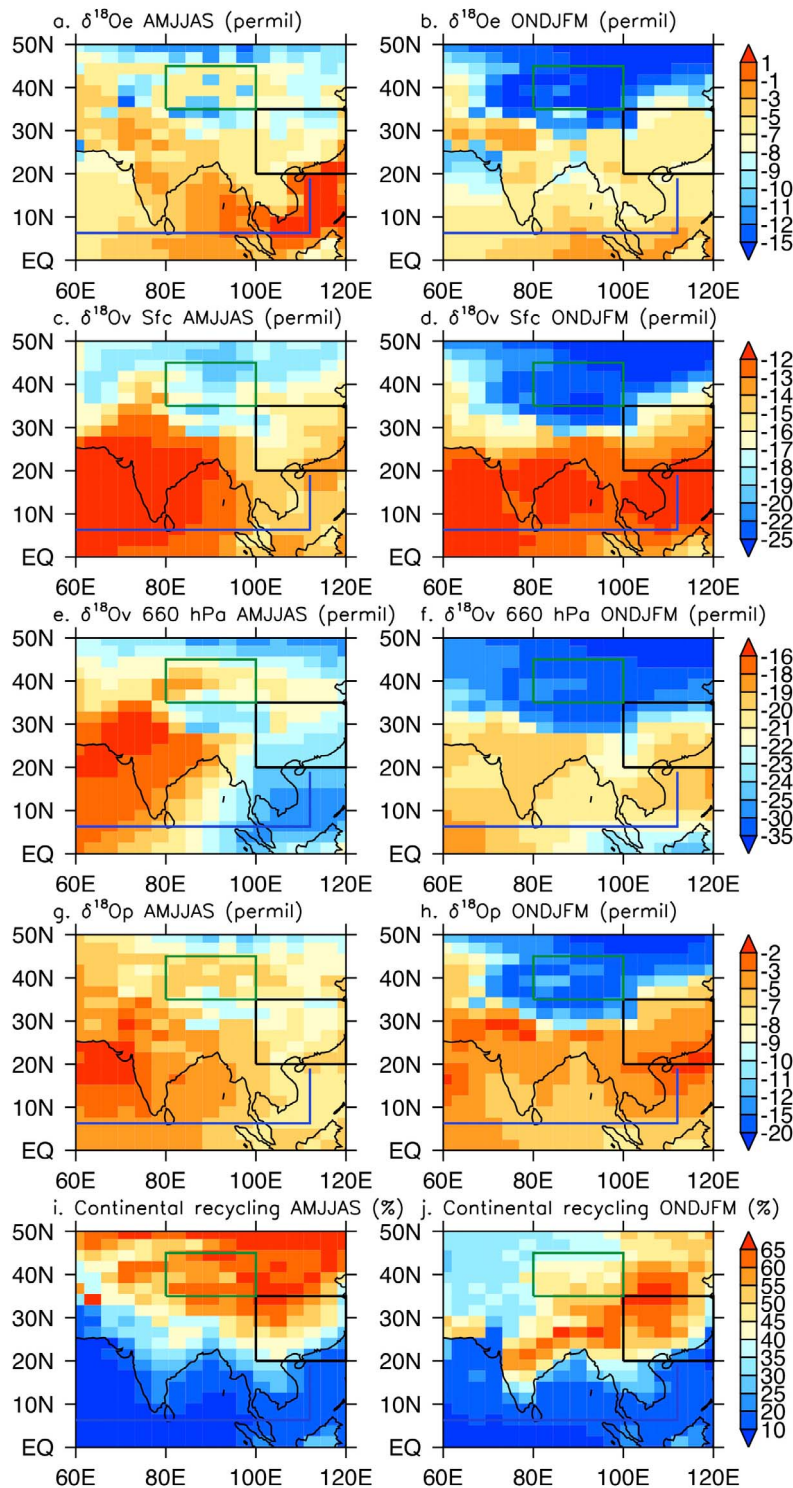
Figure 3. (a and b) LMDZ-simulated mean seasonal $\delta^{18}O$ of evaporation, (c and d) near-surface vapor, (e and f) mid-tropospheric vapor, and (g and h) precipitation, and (i and j) the contribution (%) of precipitation coming from continental evapotranspiration for summer (JJA; left column) and during winter (DJF; right column).

vapor as it falls and thus retains the isotopic signature of the condensation level. In addition, winter evapotranspiration in the continental interior is minimal. As an air mass moves inland beyond Xian, precipitation should reduce the

remaining $\delta^{18}O_v$, and thus $\delta^{18}O_p$ values decrease as temperature decreases.

[16] From Hong Kong (22°N) to Guiyang (26°N), $\delta^{18}O_p$ remains relatively constant at approximately −4 ‰ despite a
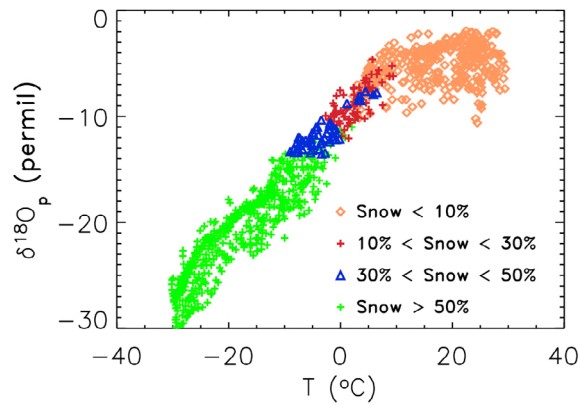
Figure 4. The relationship between temperature (°C) and $\delta^{18}O_p$ (‰) over Eurasia depending on the proportion of snow to the total precipitation during winter (DJF). Since snow output is not available from the LMDZ model, we used the National Center for Atmospheric Research (NCAR) Community Atmospheric Model Version 2 forced by climatologically fixed sea surface temperature (CAM2) [*Lee et al.*, 2007].

temperature decrease of ~13°C (from 18 to 5°C). SE China is located in the subtropics, with mean winter temperatures above 0°C and considerable winter evapotranspiration (Figure 2f). In addition, since the winter prevailing winds are offshore, a large proportion of precipitation originates from upstream regions with continental evapotranspiration with $\delta^{18}O_e$ of −4‰, which enriches $\delta^{18}O_v$ in the lower troposphere (Figures 3b and 3j).

[17] For precipitation in liquid form, falling raindrops interact with enriched vapor in the lower atmosphere and lose a large part of the isotopic signature acquired at the condensation height [*Lee and Fung*, 2008; *Field et al.*, 2010]. Thus, conditions under which precipitation consists of <10% snow exhibit only weak (r = 0.36) correlation between temperature and $\delta^{18}O_p$ (Figure 4), even during December–February when the temperature effect is known to work well [see *Rozanski et al.*, 1993]. On the other hand, for winter precipitation consisting of >50% snow, mean winter temperature and $\delta^{18}O_p$ exhibit a strong linear relationship (r = 0.91). The correlation between the mean annual temperature and mean $\delta^{18}O_p$ at different locations is high from 0 to 15°C [*Rozanski et al.*, 1993] because the mean annual temperature is related to how much snow contributes to the total precipitation [*Field*, 2010].

3.2. Summer Conditions

[18] The amount effect has been invoked to explain the variability of $\delta^{18}O_p$ over tropical and monsoon regions at multiple locations [e.g., *Dansgaard*, 1964; *Rozanski et al.*, 1993]. To assess whether $\delta^{18}O_p$ is a good indicator of the local precipitation amount over SE China [e.g., *Pausata et al.*, 2011], we compare precipitation amounts and $\delta^{18}O_p$ over upstream regions of SE China from LMDZ results (Figure 5) following the water vapor transport pathway highlighted in Figure 3 (blue line). Although $\delta^{18}O_p$ is generally low (<−6‰) over regions with high precipitation rates (>8 mm/day), Figure 5c reveals that $\delta^{18}O_p$ is not well correlated with precipitation amount when $\delta^{18}O_p$ is low. The $\delta^{18}O_p$ gradually decreases from −3‰ in the western Indian

Ocean to −7‰ in the western Pacific Ocean and South China Sea (south of black box in Figure 2). The gradual decrease of $\delta^{18}O_p$ from −3 to −7‰ to the lowest $\delta^{18}O_p$ of −8‰ over the downstream regions of strong moisture convergence (western Pacific Ocean and South China Sea) suggest that the condensation history of an air mass, not just the local precipitation amount, plays an important role in determining $\delta^{18}O_p$. Thus, $\delta^{18}O_p$ over SE China is low because of the large condensation rates over the upstream region.

[19] Next, we focus on the difference between SE and NW China at two different heights—mid-troposphere around 600 hPa where TES data are sensitive and lower troposphere where SCIAMACHY data are sensitive. We note again that the satellite retrievals of δD are more reliable than $\delta^{18}O$ and thus we analyze the former here; the δD variations are approximately 8 times larger than $\delta^{18}O$ variations. As mid-tropospheric temperatures are near or below 0°C, there is little post-condensation fractionation, so δD_v is determined by vertical mixing, the isotopic composition of transported vapor, and condensation amount. The lowest $\delta^{18}O_v$ values in the mid troposphere occur in regions where local and upstream condensation decreases δD_v, such as observed by TES data and simulated by the LMDZ4 model over the South China Sea (Figures 6a and 6b). As the air mass moves

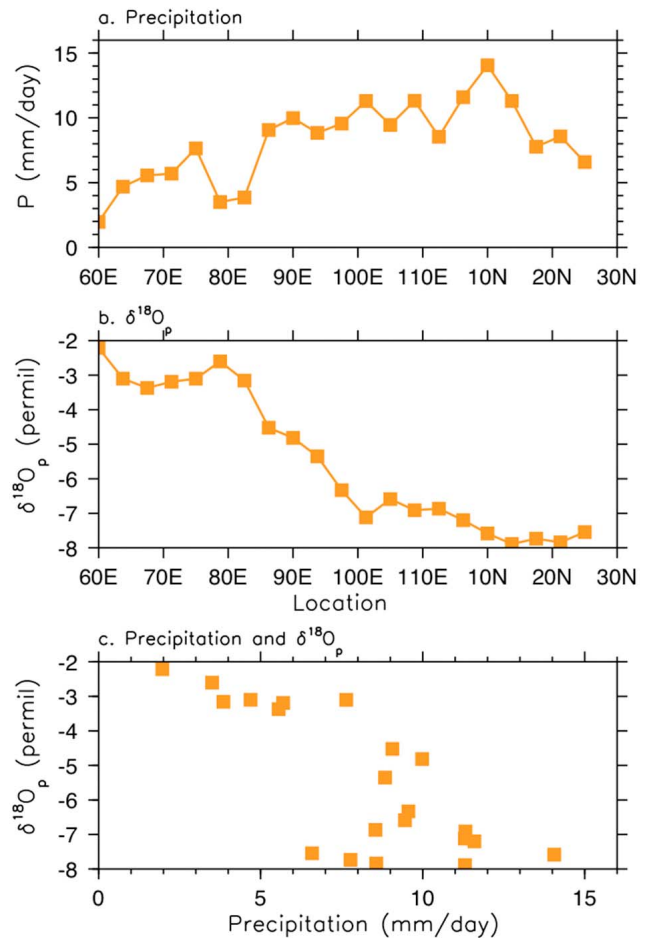**Figure 5.** (a) Mean seasonal (JJA) precipitation (mm/day), (b) $\delta^{18}O_p$ (‰), and (c) their relationship over the upstream regions of SE China along the blue line in Figure 2.
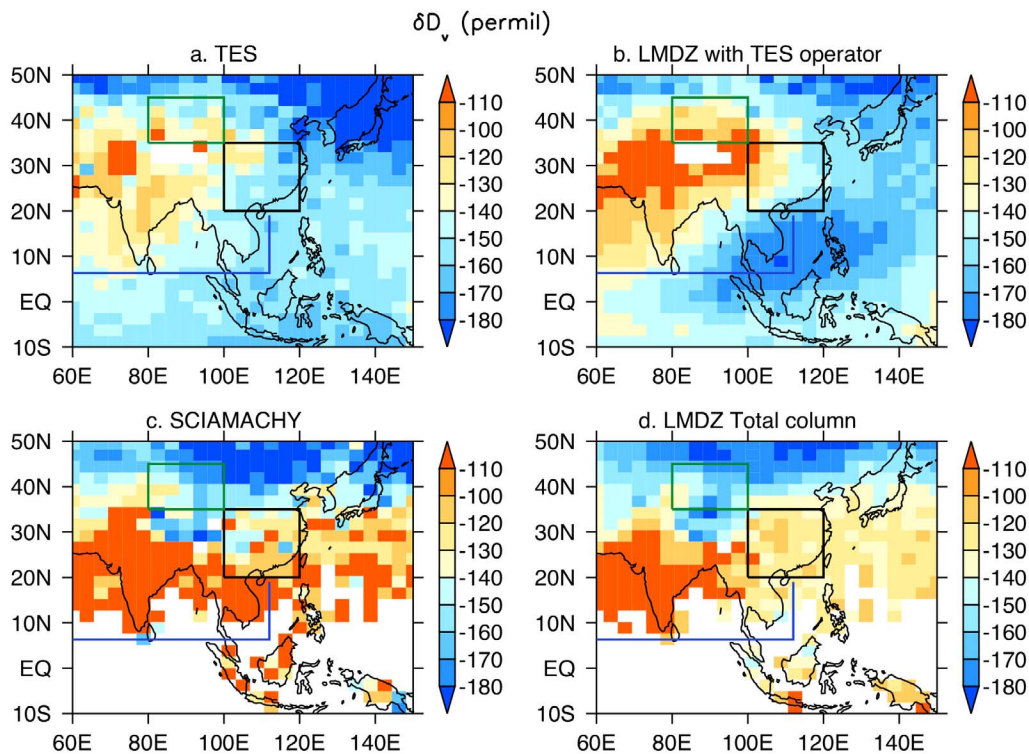
Figure 6. Mean isotopic composition in atmospheric vapor for the wet season (JJA) from (a) TES, (b) LMDZ at mid-troposphere obtained using TES operator (how TES instruments would see δD if δD in the atmosphere were distributed the same as the LMDZ simulation results), (c) SCIAMACHY, and (d) LMDZ total column for the wet season (JJA). We regridded satellite data to the LMDZ grid and sampled LMDZ results only for the day when satellite measurements are available. We added +30‰ to both TES and SCIAMACHY data.

onshore from the South China Sea, the precipitation amount decreases, yet δD_v does not increase. Over SE China, surface evapotranspiration is comparable to evaporation over the South China Sea, but $\delta^{18}O_e$ is much lower compared with the values over the South China Sea (Figure 3a). $\delta^{18}O_e$ of evapotranspiration over land is similar to the previous precipitation $\delta^{18}O$ and is not as high as $\delta^{18}O_e$ over the South China Sea because a steep ocean-atmosphere gradient of ^{18}O over the South China Sea increases $\delta^{18}O_e$ [see *Lee et al.*, 2007]. As a result, evapotranspiration over land does not enrich the vapor as much as evaporation over the South China Sea, which in turn contributes to relatively lower $\delta^{18}O_v$ over SE China. On the other hand, because the air mass over NW China originates from the arid west without much rainout (Figure 2a), $\delta^{18}O_v$ is higher than over SE China [see *Aragúas-Aragúas et al.*, 1998].

[20] Unlike precipitation or mid-tropospheric δD_v, observed δD_v in the lower troposphere from SCIAMACHY is higher over SE China than over NW China in summer (Figure 6c). Since condensation does not usually occur near the surface, surface vapor becomes depleted in heavier isotopes by diffusion as raindrops travel from the cloud base to ground [*Lee and Fung*, 2008; *Worden et al.*, 2007; *Yoshimura et al.*, 2011] and by mixing with subsiding air during convection [*Risi et al.*, 2008]. Over SE China where evapotranspiration is high, the lower tropospheric air is moister and $\delta^{18}O_v$ is higher than over NW China (Figures 3c, 6c, and 6d). Over SE China, the difference between observed

δD_p and δD_v is close to $\sim$80‰ (Figure 7). Whereas LMDZ4 results show a large *relative* contribution from land region evapotranspiration to precipitation over NW China (Figure 3i), the *absolute* magnitude of evapotranspiration is small (Figure 2e) and tropospheric specific humidity is low because the soil is dry. Thus the enrichment of $\delta^{18}O_v$ by evapotranspiration is minimal. More depleted $\delta^{18}O_v$ from the SCIAMACHY observations over NW China refute the hypothesis that large evapotranspiration contributes to the high $\delta^{18}O_p$ there.

[21] Figure 7 provides a brief summary of our findings. Since lower tropospheric vapor is more depleted in heavy isotopes over NW China compared with SE China, the question of why NW China has higher δD_p and $\delta^{18}O_p$ remains. The δD of near surface vapor from SCIAMACHY over NW China is $\sim$−156‰ after the bias correction discussed in section 2 is applied (Figure 6c). Rainfall in equilibrium with this vapor would have δD_p of $\sim$−76‰. However, the mean observed (GNIP) δD_p is $\sim$−26‰, implying that a non-equilibrium process is involved. As raindrops fall through unsaturated air below the cloud base, $H_2^{16}O$ evaporates faster than HDO or $H_2^{18}O$ because the diffusivity of $H_2^{16}O$ is higher than that of HDO, thus increasing δD_p [*Dansgaard*, 1964; *Stewart*, 1975; *Lee and Fung*, 2008]. Although bias corrections have been applied here to the LMDZ4 simulation (see section 2), these do not change our conclusion since uncorrected δD_v will have an even larger difference from δD_p.
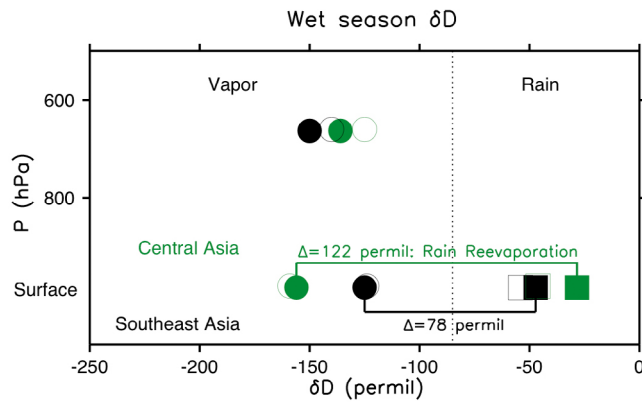
Figure 7. Mean isotopic composition of vapor (circles) and precipitation (squares) for NW (green; 35°N–45°N and 90°E–100°E; green box in Figure 2) and SE China (black; 20°N–35°N, 110°E–120°E; black box in Figure 2) during the wet season (JJA). Filled symbols represent measurements and open symbols represent LMDZ simulations. Vapor values are obtained from satellite measurements (SCIAMACHY for the low tropospheric vapor); precipitation values are from GNIP data over Guiyang (SE China) and Zhangye (NW China). At equilibrium, δD_p is ~80‰ higher than δD_v. Over NW China, the difference between δD_p and low tropospheric δD_v is large because re-evaporation of rainfall in the atmosphere increases δD_p. We added +30‰ to both TES and SCIAMACHY data.

[22] To demonstrate that rain re-evaporation is responsible for the wet-season isotope gradient, we performed an additional simulation without fractionation during rain re-evaporation. This is the same as the *Field et al.* [2010] experiment without post-condensation effect. The increasing isotope trend toward NW China disappears in this run (Figure 8), confirming that the isotope gradient can be explained by rainfall re-evaporation in the model.

4. Implications for Paleoproxy Interpretation

[23] Previous studies have found a high correlation between speleothem $\delta^{18}O_p$ and millennial timescale climate forcings, i.e., insolation on orbital timescales or abrupt climate changes such as Heinrich events [e.g., *Wang et al.*, 2001, 2008]. Based on the agreement between LMDZ4 and satellite and in situ isotope measurements, we can use LMDZ results to explore how $\delta^{18}O_p$ at various well-known cave sites is related to local and/or regional precipitation amount in current climate. Interpretation of paleoproxy data is often challenging because it may be unclear whether the data reflect local or remote climatic conditions; the analysis here may provide some useful guidance for separating these.
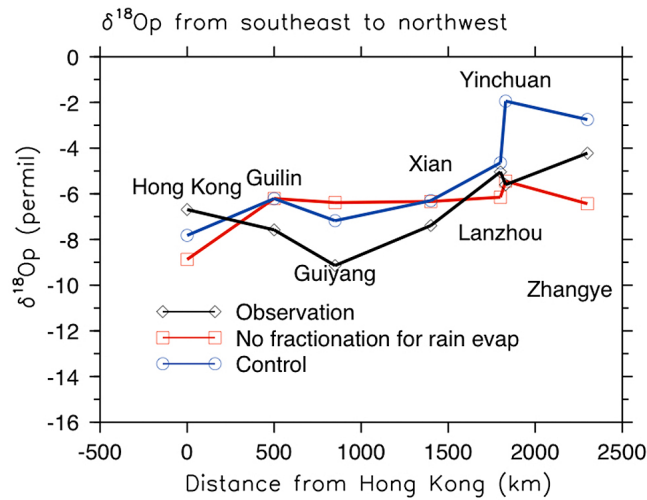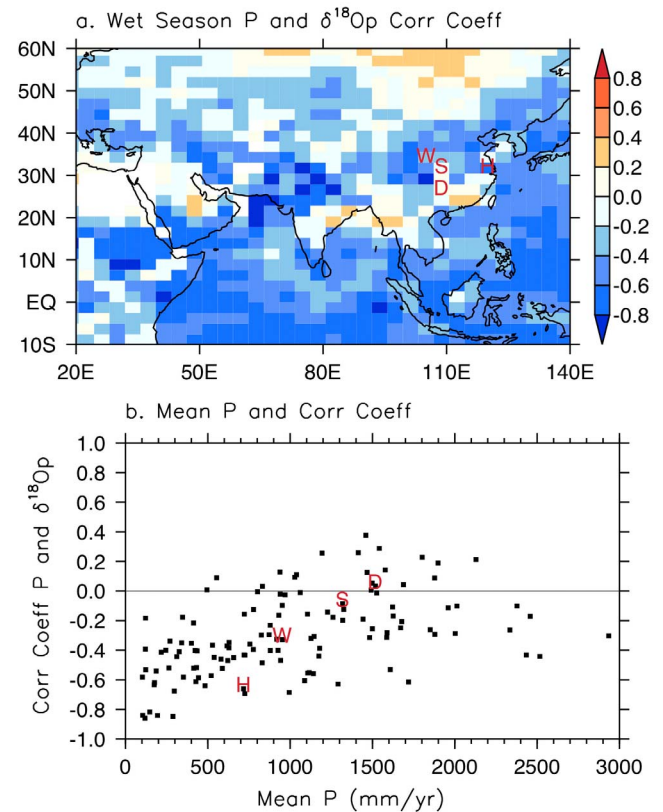

Figure 8. The role of rain re-evaporation on the isotopic gradient from Hong Kong to Zhangye. The values are from model simulation results over the GNIP stations and are calculated in the same way as Figure 1. The blue line represents results from the run with fractionation (control) and the red line represents results from the run without fractionation during rain re-evaporation for year 2009. Values from control case look different from Figure 1 because this is the summer average for year 2009 whereas Figure 1 is the summer average for the 1958–2009. The results from the run without fractionation have much smaller isotopic gradient from coastal to inland regions.

Figure 9. (a) Correlation coefficient (*r*) between wet season (April to September) precipitation amount and $\delta^{18}O_p$. H, W, S and D represent the location of Hulu, Wanxiang, Songjia, and Dongge cave sites. (b) The relationship between mean precipitation (mm/yr) and correlation from Figure 9a over the Asian monsoon region (60°E–120°E, 10°N–40°N and over land). Regions with precipitation lower than 100 mm/year are excluded. The correlation coefficient between *r* and mean precipitation from Figure 9b is 0.47.
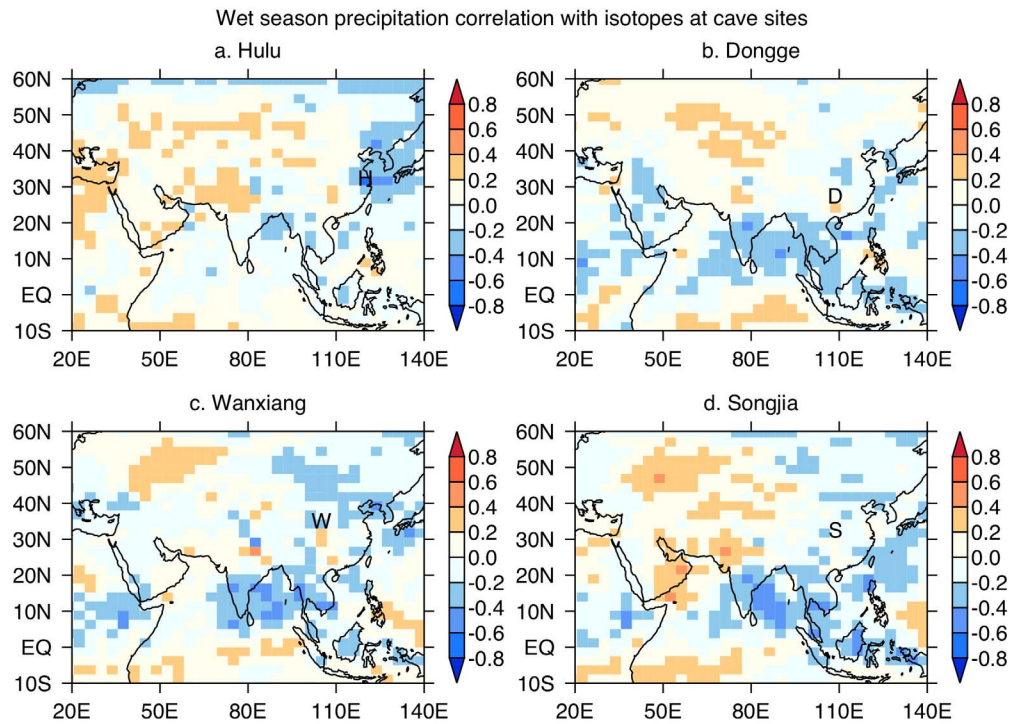
Figure 10. Correlation coefficient (r) between wet season (April to September) $\delta^{18}O_p$ over cave sites ((a) Hulu, (b) Dongge, (c) Songjia, and (d) Wanxiang) and precipitation at each grid point. H, W, S and D represent the location of cave sites. The $\delta^{18}O_p$ values from Dongge, Songjia, and Wanxiang cave sites are related with precipitation over the Indian monsoon region, and not local precipitation. Hulu cave $\delta^{18}O_p$ are related with local and more eastern part precipitation.

[24] To show how $\delta^{18}O_p$ responds to climate forcing, we calculate the correlation coefficient (r) between mean wet season (April to September) precipitation amount and $\delta^{18}O_p$ from 1958 to 2009 using LMDZ4 simulation results (Figure 9). Over oceanic regions, isotope values reflect high negative correlations with local precipitation amount [*Dansgaard*, 1964; *Rozanski et al.*, 1993]. Because local evaporation has much higher $\delta^{18}O_v$ compared with vapor transported from other areas, increasing moisture convergence (hence increasing precipitation) lowers $\delta^{18}O_v$ [*Lee et al.*, 2007]. If the changes associated with converging vapor $\delta^{18}O_v$ are small, $\delta^{18}O_p$ can be used to infer local precipitation amount changes [*Lee et al.*, 2009a]. For regions downstream of highly convective areas, local $\delta^{18}O_p$ changes come from either the amount of convergence or converging vapor $\delta^{18}O_v$, and thus the amount effect may not work well, consistent with observed GNIP isotope behavior [*Dayem et al.*, 2010]. Over relatively dry areas (precipitation $<\sim$750 mm/year), the correlation is consistently negative because rain re-evaporation plays a significant role.

[25] Next, we calculate the correlation between $\delta^{18}O_p$ at cave sites and precipitation amounts at each grid point from 1958 to 2009 (Figure 10) to assess the extent to which $\delta^{18}O_p$ at cave sites is sensitive to remote precipitation changes. As is obvious from Figure 9, the correlation between $\delta^{18}O_p$ and local precipitation is low at the Songjia and Dongge cave sites ($r = -0.03$ and 0.09). Rather, the $\delta^{18}O_p$ values at these sites are correlated with precipitation around the Bay of Bengal, consistent with *Pausata et al.* [2011]. This implies that despite the apparent correlation between $\delta^{18}O_p$ and climate forcings

such as insolation or Heinrich events, precipitation over Southeast China may not be directly related with those forcings [e.g., *Wang et al.*, 2008]. Precipitation during the wet season over southern and central China comes from the mechanical forcing related to the Tibetan Plateau [*Molnar et al.*, 2010], and thus, the convergence may not vary along with insolation changes. The Indian monsoon, on the other hand, may be more related with orbital and millennial timescale climate forcings [e.g., *Pausata et al.*, 2011], and $\delta^{18}O_p$ over southern Chinese caves probably records changes in Indian monsoon variability (Figure 10). Although $\delta^{18}O_p$ over southern China is not related to local precipitation, the $\delta^{18}O_p$ at cave sites is highly correlated with the $\delta^{18}O_p$ over large areas of southern and central China (Figure 11), consistent with high correlation of $\delta^{18}O_p$ among sites over China because isotopic changes in the upstream region are transported to the downstream region along the prevailing wind direction.

[26] The $\delta^{18}O_p$ over the more northward, drier regions of China show consistent negative correlations with local precipitation. The Hulu cave site $\delta^{18}O_p$ shows a relatively high negative correlation ($r = -0.66$) with local and nearby precipitation amount. Precipitation over the northern part of China may be more related to changes in orbital and millennial timescale climate forcings as model simulations indicate that the tropical convective boundaries tend to move poleward under warmer climates [*Frierson et al.*, 2007].

[27] Based on this correlation analysis, we expect that the following general rules can be applied to other areas: (1) high correlation between precipitation amount and $\delta^{18}O_p$
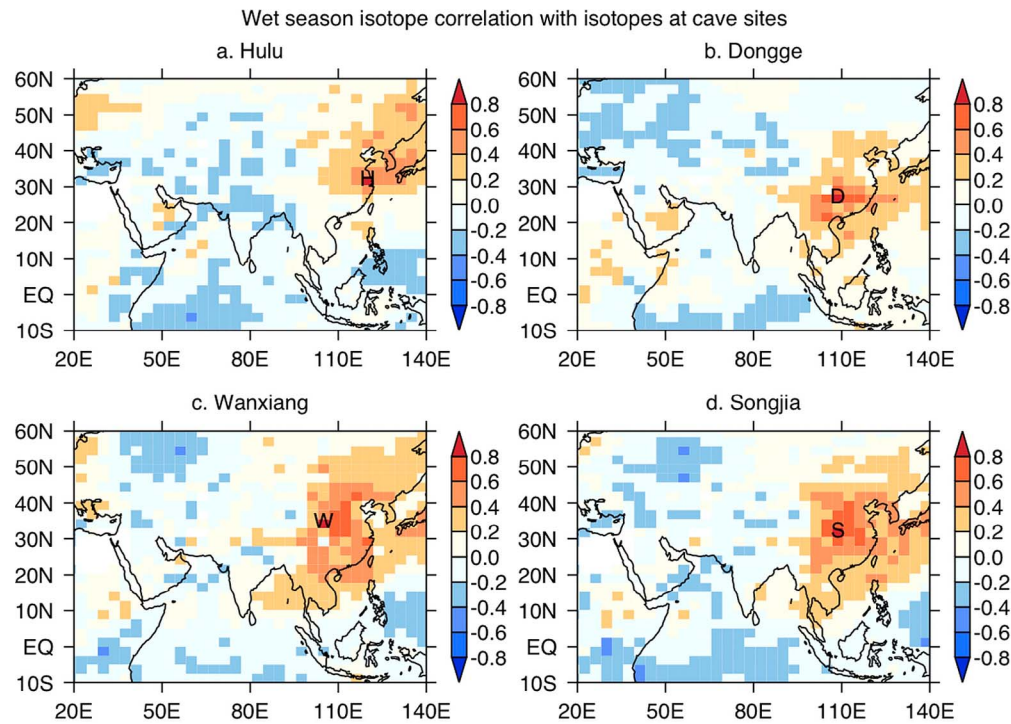
Wet season isotope correlation with isotopes at cave sites

Figure 11. Correlation coefficient (r) between wet season (April to September) $\delta^{18}O_p$ over cave sites ((a) Hulu, (b) Dongge, (c) Songjia, and (d) Wanxiang) and $\delta^{18}O_p$ at each grid point. H, W, S and D represent the location of cave sites. Although $\delta^{18}O_p$ over southern China are not related with local precipitation, it is highly correlated with regional $\delta^{18}O_p$.

over oceans and relatively dry land regions, (2) low correlation over downstream area of strong convection, and (3) high correlation between $\delta^{18}O_p$ at cave sites and $\delta^{18}O_p$ over surrounding regions. Of course, direct application of our results to paleoproxy interpretation warrants some caution because speleothems (or other proxies) record isotopic responses to millennial timescale with different background climate states whereas our results only show isotopic responses to recent interannual variations. Also, seasonality changes in precipitation are relatively small on current day, interannual timescales but may be larger on longer timescales [*Clemens et al.*, 2010].

5. Summary and Conclusion

[28] In this study, we explore controls on $\delta^{18}O_p$ over Asia, focusing on the contrast between SE China and NW China. Observations from GNIP indicate that $\delta^{18}O_p$ increases from coastal SE China toward the continental interior of NW China during summer, with data from the TES and SCIA-MACHY satellite confirming this increase. Simulations performed with an isotope-enabled version of the LMDZ model suggest that $\delta^{18}O_p$ is high over NW China because of re-evaporation of raindrops below cloud base due to the dry conditions there and the faster diffusion of ^{16}O relative to ^{18}O. Further, the SCIAMACHY measurements show low near-surface $\delta^{18}O_v$ despite high $\delta^{18}O_p$, indicating that local evapotranspiration is too small to affect specific humidity or $\delta^{18}O_v$. Over SE China, $\delta^{18}O_p$ is low during the wet season because the Southern Tibetan Plateau deflects westerly wind

and induces downstream moisture convergence [*Wu et al.*, 2007; *Molnar et al.*, 2010; *Park et al.*, 2012] of low $\delta^{18}O_v$.

[29] Our results suggest that $\delta^{18}O_p$ changes over southern China may not be related to the local precipitation response to insolation or abrupt climate changes such as Heinrich events despite the apparent high correlation between $\delta^{18}O_p$ and climate changes [e.g., *Wang et al.*, 2008]. However, if the changes in proxy $\delta^{18}O_p$ between two periods are of the same sign over a large area, large changes of precipitation probably occurred over a wide area of the upstream regions of proxy sites. By contrast, the $\delta^{18}O_p$ changes in northern China will be strongly affected by aridity of the area and local precipitation because relative humidity is low under low precipitation conditions. We suggest that precipitation over the northern part of China may be more related to changes in orbital and millennial timescale climate forcings as model simulations indicate that the tropical convective boundaries tend to shift poleward under warmer climates [see *Frierson et al.*, 2007].

References

Annamalai, H., K. Hamilton, and K. R. Sperber (2007), South Asian Summer Monsoon and its relationship with ENSO in the IPCC AR4 simulations, *J. Clim.*, 20, 1071–1092, doi:10.1175/JCLI4035.1.

Aragúas-Aragúas, L., K. Froehlich, and K. Rozanski (1998), Stable isotope composition of precipitation over Southeast Asia, *J. Geophys. Res.*, 103, 28,721–28,742, doi:10.1029/98JD02582.

Clemens, S. C., W. L. Prell, and Y. Sun (2010), Orbital-scale timing and mechanisms driving Late Pleistocene Indo-Asian summer monsoons: Reinterpreting cave speleothem d18O, *Paleoceanography*, 25, PA4207, doi:10.1029/2010PA001926.

Craig, H., and L. I. Gordon (1965), Deuterium and oxygen 18 variations in the ocean and the marine atmosphere, in *Stable Isotopes in Oceanographic Studies and Paleotemperatures*, edited by E. Tongiorgi, pp. 9–130, Lab. di Geol. Nucl., Pisa, Italy.

Dansgaard, W. (1964), Stable isotopes in precipitation, *Tellus*, 16, 436–468, doi:10.1111/j.2153-3490.1964.tb00181.x.

Dawson, T. E., and J. R. Ehleringer (1998), Plants, isotopes and water use: A catchment-scale perspective, in *Isotope Tracers in Catchment Hydrology*, edited by C. Kendall and J. J. McConnell, pp. 165–202, Elsevier Sci., Amsterdam.

Dayem, K. E., D. S. Battisti, G. H. Roe, and P. Molnar (2010), Lessons learned from oxygen isotopes in modern precipitation applied to interpretation of speleothem records of paleoclimate from eastern Asia, *Earth Planet. Sci. Lett.*, 295, 219–230, doi:10.1016/j.epsl.2010.04.003.

Field, R. D. (2010), Observed and modeled controls on precipitation δ^{18}O over Europe: From local temperature to the Northern Annular Mode, *J. Geophys. Res.*, 115, D12101, doi:10.1029/2009JD013370.

Field, R. D., D. B. A. Jones, and D. P. Brown (2010), Effects of postcondensation exchange on the isotopic composition of water in the atmosphere, *J. Geophys. Res.*, 115, D24305, doi:10.1029/2010JD014334.

Frankenberg, C., et al. (2009), Dynamic processes governing lower-tropospheric HDO/H$_2$O ratios as observed from space and ground, *Science*, 325, 1374–1377, doi:10.1126/science.1173791.

Frierson, D. M. W., J. Lu, and G. Chen (2007), Width of the Hadley cell in simple and comprehensive general circulation models, *Geophys. Res. Lett.*, 34, L18804, doi:10.1029/2007GL031115.

Gao, J., V. Masson-Delmotte, T. Yao, L. Tian, C. Risi, and G. Hoffmann (2011), Precipitation water isotopes in the South Tibetan Plateau: Observations and modeling, *J. Clim.*, 24, 3161–3178, doi:10.1175/2010JCLI3736.1.

Garzione, C. N., P. Molnar, J. C. Libarkin, and B. J. MacFadden (2006), Rapid late Miocene rise of the Bolivian Altiplano: Evidence for removal of mantle lithosphere, *Earth Planet. Sci. Lett.*, 241, 543–556, doi:10.1016/j.epsl.2005.11.026.

Hendricks, M. B., D. J. DePaolo, and R. C. Cohen (2000), Space and time variation of δ^{18}O and δD in precipitation: Can paleotemperature be estimated from ice cores?, *Global Biogeochem. Cycles*, 14, 851–861, doi:10.1029/1999GB001198.

Hourdin, F., et al. (2006), The LMDZ4 general circulation model: Climate performance and sensitivity to parametrized physics with emphasis on tropical convection, *Clim. Dyn.*, 27, 787–813, doi:10.1007/s00382-006-0158-0.

Koster, R., J. Jouzel, R. Suozzo, G. Russell, W. Broecker, D. Rind, and P. Eagleson (1986), Global sources of local precipitation as determined by the NASA GISS GCM, *Geophys. Res. Lett.*, 13, 121–124, doi:10.1029/GL013i002p00121.

Kurita, N., and H. Yamada (2008), The role of local moisture recycling evaluated using stable isotope data from over the middle of the Tibetan Plateau during the monsoon season, *J. Hydrometeorol.*, 9, 760–775, doi:10.1175/2007JHM945.1.

Lee, J.-E., and I. Fung (2008), "Amount effect" of water isotopes and quantitative analysis of post-condensation processes, *Hydrol. Processes*, 22, 1–8, doi:10.1002/hyp.6637.

Lee, J.-E., I. Fung, D. J. DePaolo, and C. C. Henning (2007), Analysis of the global distribution of water isotopes using the NCAR atmospheric general circulation model, *J. Geophys. Res.*, 112, D16306, doi:10.1029/2006JD007657.

Lee, J.-E., I. Fung, D. J. DePaolo, and B. Otto-Bliesner (2008), Water isotopes during the Last Glacial Maximum: New general circulation model calculations, *J. Geophys. Res.*, 113, D19109, doi:10.1029/2008JD009859.

Lee, J.-E., K. Johnson, and I. Fung (2009a), Precipitation over South America during the Last Glacial Maximum: An analysis of the "amount effect" with a water isotope-enabled general circulation model, *Geophys. Res. Lett.*, 36, L19701, doi:10.1029/2009GL039265.

Lee, J.-E., R. Pierrehumbert, A. Swann, and B. R. Lintner (2009b), Sensitivity of the stable water isotopic values on the convective parameterization schemes, *Geophys. Res. Lett.*, 36, L23801, doi:10.1029/2009GL040880.

Molnar, P., W. R. Boos, and D. S. Battisti (2010), Orographic controls on climate and paleoclimate of Asia: Thermal and mechanical roles for the Tibetan Plateau, *Annu. Rev. Earth Planet. Sci.*, 38, 77–102, doi:10.1146/annurev-earth-040809-152456.

Park, H.-S., J. Chiang, and S. Bordoni (2012), Mechanical impact of the Tibetan Plateau on the seasonal evolution of the South Asian Monsoon, *J. Clim.*, 25, 2394–2407, doi:10.1175/JCLI-D-11-00281.1.

Pausata, F. S. R., D. Battisti, K. Nisancioglu, and C. M. Bits (2011), Chinese stalagmite δ^{18}O controlled by changes in the Indian monsoon during a simulated Heinrich event, *Nat. Geosci.*, 4, 474–480, doi:10.1038/ngeo1169.

Rayner, N. A., D. E. Parker, E. B. Horton, C. K. Folland, L. V. Alexander, D. P. Rowell, E. C. Kent, and A. Kaplan (2003), Global analyses of sea surface temperature, sea ice, and night marine air temperature since the late nineteenth century, *J. Geophys. Res.*, 108(D14), 4407, doi:10.1029/2002JD002670.

Risi, C., S. Bony, and F. Vimeux (2008), Influence of convective processes on the isotopic composition (δ^{18}O and δD) of precipitation and water vapor in the tropics: 2. Physical interpretation of the amount effect, *J. Geophys. Res.*, 113, D19306, doi:10.1029/2008JD009943.

Risi, C., S. Bony, F. Vimeux, and J. Jouzel (2010a), Water stable isotopes in the LMDZ4 general circulation model: Model evaluation for present day and past climates and applications to climatic interpretation of tropical isotopic records, *J. Geophys. Res.*, 115, D12118, doi:10.1029/2009JD013255.

Risi, C., S. Bony, F. Vimeux, C. Frankenberg, D. Noone, and J. Worden (2010b), Understanding the Sahelian water budget through the isotopic composition of water vapor and precipitation, *J. Geophys. Res.*, 115, D24110, doi:10.1029/2010JD014690.

Risi, C., et al. (2012a), Process-evaluation of tropospheric humidity simulated by general circulation models using water vapor isotopologues: 1. Comparison between models and observations, *J. Geophys. Res.*, 117, D05303, doi:10.1029/2011JD016621.

Risi, C., et al. (2012b), Process-evaluation of tropospheric humidity simulated by general circulation models using water vapor isotopic observations: 2. Using isotopic diagnostics to understand the mid and upper tropospheric moist bias in the tropics and subtropics, *J. Geophys. Res.*, 117, D05304, doi:10.1029/2011JD016623.

Rowley, D. B., R. T. Pierrehumbert, and B. S. Currie (2001), A new approach to stable isotope-based paleoaltimetry: Implications for paleoaltimetry and paleohypsometry of the High Himalaya since the Late Miocene, *Earth Planet. Sci. Lett.*, 188, 253–268, doi:10.1016/S0012-821X(01)00324-7.

Rozanski, K., L. Aragúas-Aragúas, and R. Gonfiantini (1993), Isotopic patterns in modern global precipitation, in *Climate Change in Continental Isotopic Records*, *Geophys. Monogr. Ser*, vol. 78, edited by P. K. Swart et al., pp. 1–36, AGU, Washington, D. C., doi:10.1029/GM078p0001.

Stewart, M. K. (1975), Stable isotope fractionation due to evaporation and isotopic-exchange of falling waterdrops: Applications to atmospheric processes and evaporation of lakes, *J. Geophys. Res.*, 80, 1133–1146, doi:10.1029/JC080i009p01133.

Sturm, K., G. Hoffmann, B. Langmann, and W. Stichler (2005), Simulation of δ^{18}O in precipitation by the regional circulation model REMOiso, *Hydrol. Processes*, 19, 3425–3444, doi:10.1002/hyp.5979.

Uppala, S., et al. (2005), The ERA-40 re-analysis, *Q. J. R. Meteorol. Soc.*, 131, 2961–3012, doi:10.1256/qj.04.176.

Wang, Y. J., H. Cheng, R. L. Edwards, Z. S. An, J. Y. Wu, C. C. Shen, and J. A. Dorale (2001), A high-resolution absolute-dated late Pleistocene monsoon record from Hulu Cave, China, *Science*, 294, 2345–2348, doi:10.1126/science.1064618.

Wang, Y. J., H. Cheng, R. L. Edwards, X. G. Kong, X. H. Shao, S. T. Chen, J. Y. Wu, X. Y. Jiang, X. F. Wang, and Z. S. An (2008), Millennial- and orbital-scale changes in the East Asian monsoon over the past 224,000 years, *Nature*, 451, 1090–1093, doi:10.1038/nature06692.

Werner, M., P. M. Langebroek, T. Carlsen, M. Herold, and G. Lohmann (2011), Stable water isotopes in the ECHAM5 general circulation model: Toward high-resolution isotope modeling on a global scale, *J. Geophys. Res.*, 116, D15109, doi:10.1029/2011JD015681.

Worden, J., et al. (2006), Tropospheric emission spectrometer observations of the tropospheric HDO/H$_2$O ratio: Estimation approach and characterization, *J. Geophys. Res.*, 111, D16309, doi:10.1029/2005JD006606.

Worden, J., D. Noone, and K. Bowman (2007), Importance of rain evaporation and continental convection in the tropical water cycle, *Nature*, 445, 528–532, doi:10.1038/nature05508.

Worden, J., et al. (2011), Estimate of bias in Aura TES HDO/H_2O profiles from comparison of TES and in situ HDO/H_2O measurements at the Mauna Loa observatory, *Atmos. Chem. Phys.*, *11*, 4491–4503, doi:10.5194/acp-11-4491-2011.

Wu, G.-X., et al. (2007), The influence of mechanical and thermal forcing by the Tibetan Plateau on Asian climate, *J. Hydrometeorol.*, *8*, 770–789, doi:10.1175/JHM609.1.

Yoshimura, K., M. Kanamitsu, D. Noone, and T. Oki (2008), Historical isotope simulation using reanalysis atmospheric data, *J. Geophys. Res.*, *113*, D19108, doi:10.1029/2008JD010074.

Yoshimura, K., C. Frankenberg, J. Lee, M. Kanamitsu, J. Worden, and T. Röckmann (2011), Comparison of an isotopic AGCM with new quasi global satellite measurements of water vapor isotopologues, *J. Geophys. Res.*, *116*, D19118, doi:10.1029/2011JD016035.